ORIGINAL ARTICLE

Stress–strain parameter prediction method for AWJ technology from surface topography

Jan Valíček[1,2,3] · Marta Harničárová[1,2,3] · Milena Kušnerová[2] · Zuzana Palková[1,2] · Ivan Kopal[4] · Cristina Borzan[5] · Andrej Czán[3] · Rastislav Mikuš[6] · Milan Kadnár[6] · Stanislaw Duer[7] · Vladimír Šepelák[2,8]

Abstract

The presented publication is based on the interaction of the material core and its surface during the machining process with a hydro abrasive flexible cutting tool (AWJ). In the AWJ technology, a cold cut is generated; therefore, there are no thermal stresses on the newly formed surface and, consequently, no significant internal and residual stresses. The cut is identifiable by directly measurable parameters: depth of cut, deviation of the cut path from the normal plane, and surface roughness. These geometric parameters are interdependent at each cut zone point and simultaneously dependent on a newly proposed, indirectly measurable material parameter, K_{plmat}. Although the deviation angle of the cutting path from the normal plane increases with increasing depth of cut, the ratio of the "material plasticity" K_{plmat} and the surface roughness Ra of the cutting surface remains equivalent to the ratio of the depth of cut and the deviation of the cutting path from the normal plane. Based on the proposed concept, an entirely new approach to the problem of material surface integrity is presented by the method of identification of mechanical equivalents and their functional transformation. The solution to the subject problem is based on the fact that the technological process of machined material decomposition specifically and identically "copies" the surface properties of the material, i.e. records its technological inheritance. The material properties can then be "read retrospectively" reliably and accurately using the recording.

Keywords Surface roughness · Mechanical parameters · Abrasive waterjet · Material plasticity · Deformation

1 Introduction

Although the abrasive water jet machining process is not a novel technology and belongs to the advanced machining processes [1], it is broadly used in different areas such as the manufacturing industry [2, 3], civil and construction industry [4], mining [5], aerospace [6], military industry [7], food processing sector [8], cleaning [9], or in medicine [10].

The cutting process using an abrasive waterjet (AWJ) represents a disintegration process due to the force, stress, and deformation action of a cutting tool on the workpiece material. In AWJ technology, it is a machining tool with slightly different mechanical properties than conventional machining tools used for dividing, cutting, machining, or drilling. A final result of the cutting process is a cut. The topographical function of the cut wall surface finally describes the balance of cutting forces that occurs due to the mechanism of opposing external and internal interactions caused by the cutting

tool. In principle, the deformation process of material cutting in the AWJ technology is caused by a high-speed water jet carrying abrasive particles. The cut starts due to kinetic energy that converts into pressure energy.

The analysis of AWJ parameters proves that hydraulic parameters (pressure p, nozzle outlet diameter d_o) and abrasive parameters (kind of abrasive material, amount of abrasive particles a_o, mass flow rate m_a) have the most significant influence on the process of cutting materials and its effectiveness. Among the mixing parameters, diameter d_a and length l_a of the focusing tube have the most significant influence and among the group of cutting parameters for the process of AWJ cutting, the traverse rate v_p has the ultimate influence [11]. The difference between waterjet and abrasive waterjet technology is in the use of an abrasive material, for which important parameters, e.g. particle size distribution and physical, mechanical, and chemical properties, are important. Furthermore, it is necessary to monitor the effect of quality changes following the interaction of the abrasive with the processed material [12].

Extended author information available on the last page of the article

Surface treatment with abrasives was studied by Vijay Kumar Jain et al. Impingement of the abrasive particle on the workpiece surface causes extremely high stresses and these stresses cause a local plastic deformation at the site of impact [13–17].

J. G. A. Bitter was the first who dealt with a study of erosion phenomena caused by AWJ [18, 19]. Hashish continued in the study of abrasive waterjet machining. He considered into account the importance of strain rate and counted with two modes, deformation and cutting wear modes. In his model, he used the theoretical fracture strength (E/14) as a material constant to identify deformation wear mode while the yield strength was considered a measure of hardness to identify the cutting wear mode [20–23].

Shao [24] predicted surface roughness and morphology changes through micro-cutting mechanics modelling and Monte Carlo algorithms. This feasible approach can enhance the accuracy and efficiency of abrasive flow machining processes by establishing a constitutive model that accurately describes the rheological behaviour of abrasive media.

In this context, it should be emphasised that the erudite research of AWJ technology requires a deeper analysis of measurement results and their interpretation up to the level of generalisation, but most of the work focuses only on the presentation of laboratory measurement results, or on the comparison of measurement results presented by various laboratories. It should also be noted that if the interpretations of the results are already performed, the observed regular zonalities in the occurrence of analogous values of geometric and tensometric parameters identifying the position of a particular zone in the depth of cut are not respected. The zonality is a phenomenon of abrasive waterjet erosion of a surface layer, and its manifestation is equally regular as manifestations of retardation and deviation of cut trace. However, it can fully show itself only at sufficiently great depths of cutting or in prediction calculations performed for depths less than limit depths in various materials.

The quality of the machined surface is mainly evaluated by surface roughness. The selection of appropriate machining parameters affects the final surface roughness. The goal of the process is to get the surface, which does not require secondary finishing operations. The overall structure of surface topography is formed by a morphological wave as a carrying geometric structure with a higher amplitude, longer wavelength, and thus lower frequency because this type of deformation is generated by a substantial contribution of external influences (vibration of the sample of material, cutting head, and the whole construction). The final profile of the surface is an integrated structure of individual components of macroscopic waviness and microscopic roughness. In contrast to the hitherto approach, it is necessary, in our opinion, to put much greater emphasis on stress-deformation and tensometric properties of the material being cut

in relation to the mechanical stiffness of the cutting tool itself, i.e. the AWJ stream. Primary emphasis should be then placed on the study of macrotexture and microtexture of cut wall surface generated by the abrasive waterjet cutting process. The informative ability of geometric phenomena of the topography of newly generated surfaces is analytically an essential tool for the physical and mathematical formulation of both the principle of abrasive waterjet erosion of material surface layer in the cut trace and the principle of hydrodynamic and oscillation processes taking place in the disintegration system.

The shape of cuts is apparent changes with the depth of action of AWJ front below the surface of a sample being machined and is naturally an image of changes occurring in the mechanism of disintegration. With the physico-mechanical issues of interaction between the disintegration energy cumulated in AWJ and the mechanical structure of the material, many authors have been concerned [25–32]. The formed cuts are classified most simply and conventionally into the upper part of high quality, smooth cut, and from a particular critical depth to the lower part of the deformed cut. Irregularities in the upper part of the cut are qualified as microscopic and are largely of the order of roughness. Irregularities in the lower part of the cut are macroscopic; so-called striations, grooves, and irregularities of the order of waviness occur there. The depth of cut h is measured as absolute, while the depth of cut, where a relatively quick change in the mechanism of disintegration from prevailing shear to crush damage to the material due to compression occurs, is designated in the literature according to Hashish as a critical depth h_c [33–36].

Analytical relationships for the prediction of the depth in question are derived on the basis of experiments and focus on the needs of technical practice, i.e. they present dependence on technical parameters, in particular on the diameter of the nozzle and the traverse speed of cutting head, as well as on the mass flow of abrasive particles, their mass, speed of movement, and the effective proportion of particles in the cut [37–39].

According to Guo [40, 41], the attribute of the inevitable curvature of AWJ depending on the distance between its front and nozzle orifice is important to the mechanism of disintegration work. Thus, the angle of impingement α_d of abrasive particles in the AWJ cut trace changes; these authors also designated the angle corresponding to the critical depth hc as critical angle αc. The critical angle α_c of particle impingement is then, according to the authors [28, 33–41], such an angle at which the shear-cutting character of the stream changes to the deformation, pressure one, and simultaneously the cutting tool itself and the trace of its cut are curved more intensively. On the intensity of curvature, other important describing parameters for analyses depend, i.e. general angle of curvature $\delta_{gen} = f(h)$ and instantaneous

angle of curvature $\delta_i = f(h_i)$, as well as retardation of the cutting trace Y_{ret}, which is a general retardation of cut trace at the bottom of the cut $Y_{retgen} = f(h)$ and instantaneous retardation of cut trace $Y_{reti} = f(h_i)$.

The area of hydro-abrasive cutting is characterised by the retardation of the cutting path and the roughness that occurs during hydro-abrasive cutting.

A comprehensive analysis of the capabilities, recent trends, and applications of injection type AWJ machining is presented in [42]. Machining performance and surface characteristics have been compared with various engineering materials.

Research on the basic phenomena and events of AWJ technology is primarily aimed at optimising technological parameters to affect the quality of the generated cut significantly positively.

Based on the older and up to date literature [43–48] devoted to the issue of the cut wall surface quality in relation to the technological process setup for hydro-abrasive cutting technology, it is evident that the study of surface quality and the development of the topographic function during cutting is currently a much-debated issue. The analysis of literature sources indicates that the vast majority of authors use statistical, empirical, and mathematical models to quantify the various effects of technological parameters of the hydro-abrasive cutting process [49–52].

The purpose of the research in [53] was to optimise machining parameters utilised during the cutting of Hastelloy using AWJ. In order to determine the significance of parameters on measured responses, an analysis of variance (ANOVA) has been conducted. An analysis of variance revealed that water jet pressure played an increasingly important role in determining kerf width and MRR, rather than abrasive flow rate and standoff distance.

It is clear that most of the scientific research results of these publications are based on regression analysis.

Critically, it can be concluded that most of the procedures developed so far are questionable in terms of applicability in operational practice. It is mainly due to the problematic determination of a number of constants used to specify the inputs to the derived relationships.

Deformation processes in the material are the subject of interest in many scientific works. There are many mathematical models developed to predict stress–strain behaviour of a material subjected to a specific load. The most often used models are bounding surface models, the elastic, and hyperbolic models [54–56].

A conspicuous external feature of plastic deformation is an irreversible change. The macrostructural mechanical properties of loaded materials are related to processes at the micro-level of the material, and relatively simple stress–strain and strain–time formulas are used to determine them. Individual particles are collectively rearranged into new positions of internal balance. Simulation tools based on dislocation physics and finite element analysis are most often used to identify this process. Their disadvantage is that they are very time-consuming numerical tools [57–62].

A detailed knowledge of materials behaviour under external stresses is very important mainly from the point of view of safety.

The proposed solution aims to clarify the technology of hydro-abrasive cutting, especially in terms of the resulting surface topography. It provides a new perspective on the deformation process caused by the effect of hydro-abrasive cutting. It shows new possibilities for the use of surface topography in solving the issues of stress–strain relations in deformation. There is an increasing requirement to cut or otherwise machine structural materials with superior performance properties, i.e. structural materials with specific mechanical, physical, and chemical properties. The design and management of technology can no longer be based on subjective decisions but must become increasingly sophisticated; it will be forced to use exact decision-making procedures and the rapid operational capabilities of interactive mathematical modelling methods and techniques for technological processes to an ever-greater extent than hitherto. The laws of rapid evolution in the needs of practice place new demands on research and adequate theoretical support. An important role is played by the discovery of ever new possibilities for the rapid application of scientific and technical knowledge in practice.

In addition to presenting technological aspects, the article also aims to present new possibilities of using analytical processing of specific elements of surface topography generated by flexible machining tools. The hitherto neglected structure and texture of surfaces generated in this way is, in fact, an accurate representation of the physical–mechanical reaction of the material stressed by this type of tool. This aspect is theoretically generally recognised at a qualitative level, but its quantified analytical treatment and description has not yet been achieved in practice. In the presented publication, therefore, the method of derivation of a number of basic physical–mechanical parameters, or their equivalents, is elaborated transparently and in detail based on the laws of generation of structure and texture of surfaces machined with a flexible tool.

Accurate knowledge of the surface topography generated by the AWJ technology is very important in terms of its application because it allows, among other things, accurate setting of the required input parameters of the technological process. The main cause of stress in the workpiece is the plastic deformation generated in the cutting zone. Stresses in the core and surface layers of the material affect the material properties of the workpiece, especially the fatigue limit and service life. The newly introduced K_{plmat} parameter is used to determine the equivalent mechanical parameters of materials in the elastic and plastic deformation region, including numerical and

graphical parameters for engineering and realistic σ-ε diagrams, including the determination of deformation limits and their prediction for different types of materials. The method of determining equivalent mechanical parameters of materials from surface topography produced by a flexible cutting tool is advantageous for several reasons. It allows simple, inexpensive, express, and accurate determination of mechanical equivalents of material parameters in an analytical manner. It also offers easy and reliable online operational control of the mechanical parameters of all types of cut materials.

This paper aims to give a novel concept of the identification of σ-ε diagrams from the topography of functionally stressed surfaces, which has a certain attractive features of simplicity for use.

2 Theoretical background

2.1 Main geometric parameters of the topography of the cut walls

Geometric indices provide reliable information about the changes in the shape and dimensions of a permanently deformed body. The most important geometric indicators include the permanent deformations measurable on the cut wall surfaces. Permanent deformations evaluate the process qualitatively (change in physical–mechanical properties) and quantitatively (change in external dimensions). The following parameters have been proposed as the main elements of the cut wall geometry: surface roughness Ra, cutting path retardation Y_{ret}, cutting path curvature angle δ (deviation), and cutting depth h or thickness of the cut sample (Fig. 1).

Based on these selected fundamental geometrical parameters, further described parameters, and their relationships, it is possible to observe and theoretically predict the course of deformation and formation of the surface topography of the material divided by the hydro-abrasive current, not only on the spatial but also on the time scale.

Using the above conclusions and derived relations, an algorithmic procedure for the construction of transformation diagrams is developed (Fig. 1). The main input parameter to the computational algorithm is Young's modulus of elasticity E_{mat}, either as derived from measurements of topographic elements or given by the manufacturer or expressly determined, e.g. by ultrasonic measurement. As a result of the calculation, the stress profile in the section can be obtained as a function of the absolute depth of section h [mm] or the relative depth of section h_{rel} [-], or also as a function of the relative elongation ε [-] (respectively as $100 \cdot \varepsilon$). From the transformation diagram of the dependence of the deformation stress σ on the relative elongation ε, it is possible to read the values of significant limits, namely the tensile strength limit Rm, the yield strength Re, and the fracture strength R_f, as well as the stress courses, namely the engineering stress $\sigma_{raq(eng)}$ and the true stress $\sigma_{raq(true)}$.

2.2 Derivation of relations for the radial plane

The derivation of the relations for the radial plane using the sum functions in the modulus, stress, and strain regions A, B, and C (E_{sum}, σ_{sum}, Ra_{sum}) is carried out according to the schematic representation in Fig. 2. The basic consideration of the analytical treatment concept can be illustrated in the simplest way by the geometric similarity of the integral (sum)
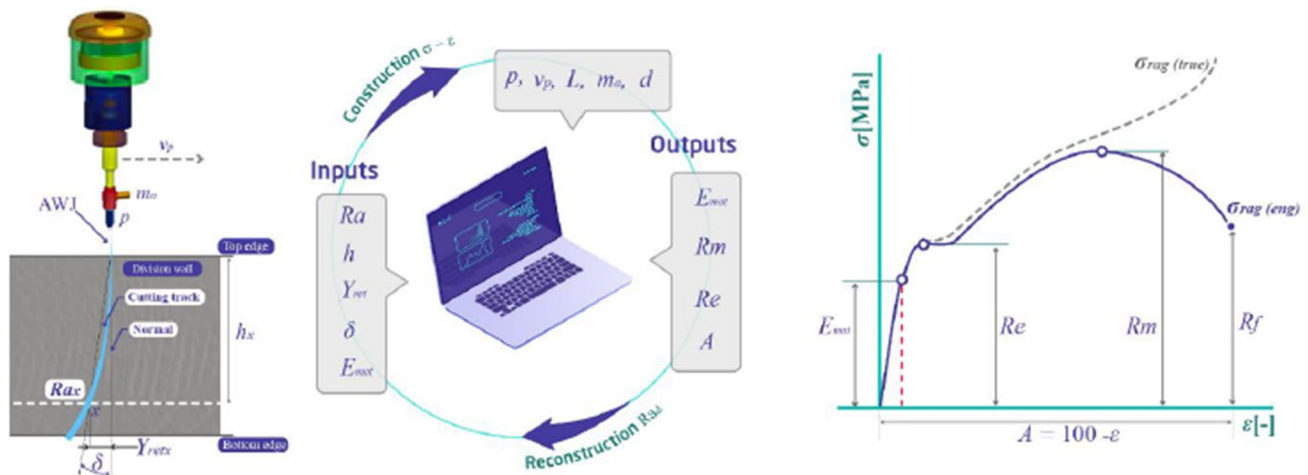

Fig. 1 Solution principle for identifying mechanical equivalents and the method of construction $\sigma - \varepsilon$, where Ra_d is the topographic function describing the surface roughness distribution Ra, p is the pressure, v_p is the cutting speed, m_a is the abrasive mass quantity, d is the diameter of the nozzle, L is the distance of the nozzle from the material to be cut, Re is the yield point, Rm is the yield point, R_f is the breaking point, $\sigma_{raq(eng)}$ is the engineering stress, and $\sigma_{raq\,(true)}$ is the true stress

Fig. 2 Stress–strain waveforms in the modulus-A, stress-B, and deformation-C region due to external stresses for AISI 304 steel material
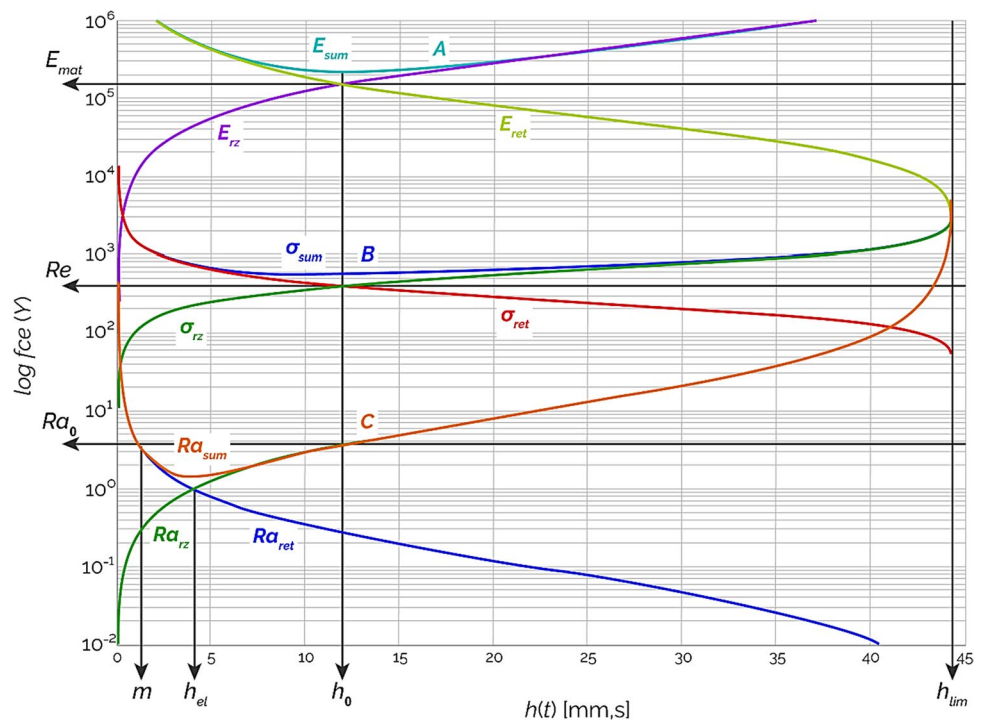
strain curves in the modulus region (A), more specifically for the evolution of material stress in the stress region (B) and for the evolution of surface roughness in the strain region (C) according to the working diagram in Fig. 2. This similarity is hypothetical and is the theoretical basis for deriving the desired relationships. The mechanism of the actual evolution of the disintegration and deformation processes corresponds well with the stress and strain distribution patterns in the investigated section. Thus, these waveforms provide information on the occurrence and evolution of tensile stresses and compressive stresses and the deformations induced by them.

Thus, additional relations (1) to (7) can be obtained for decomposing the subject quantities into tension and compression components, including their summed and neutral plane values. For the summed stresses, the relation (1) containing the stress decomposition component σ_{rz} (2) for the pressure and the retardation decomposition component (3) for the tension σ_{ret} applies.

$$\sigma_{sum} = \sqrt{(\sigma_{rz}^2 + \sigma_{ret}^2)}, \tag{1}$$

$$\sigma_{rz} = \sqrt{E_{rz}}, \tag{2}$$

$$\sigma_{ret} = \sqrt{E_{ret}} \tag{3}$$

In Eqs. (4) to (5), the material parameters are the tensile modulus E_{mat}, its decomposition components for pressure E_{rz}, for tension E_{ret}, and the transverse surface plasticity

K_{pl}. The surface plasticity is defined as the instantaneous deformation region, which is given by the product of the instantaneous values of the roughness Ra and the depth h. The introduced parameters ε_{rz} and ε_{ret} in Eqs. (4) and (5) represent the relative deformations in the compressive and tensile components at the level of the modulus region (A). The parameter K_{pl} represents the deformation surface region on the section as a function of the instantaneous roughness Ra and the instantaneous depth h_{cut}.

$$E_{rz} = E_{mat} \cdot \varepsilon_{rz}, \tag{4}$$

$$E_{ret} = E_{mat} \cdot \varepsilon_{ret}, \tag{5}$$

For the relative deformations, relations (6) and (7) apply again by analogy.

$$\varepsilon_{rz} = 10^6 \cdot \frac{\varepsilon_{rz0}}{E_{mat}} \cdot \sqrt{Ra \cdot h} \tag{6}$$

$$\varepsilon_{ret} = 10^6 \cdot \frac{\varepsilon_{rz0}}{E_{mat} \cdot \sqrt{Ra \cdot h}} \tag{7}$$

Similarly, the decomposition component of the modulus of elasticity for compression and tension can also be defined for the regions in the stress level (B) and for the development of surface roughness in the decomposition level (C) in the sense of the graph in Fig. 2. This is because it is always a decomposition of the main parametric functions into their tensile or compressive components. The summed, geometric

sum of the two components is the tabulated value of the parameter. The root of relations (4) and (5) can be further extracted into the forms (8) and (9),where σ_{m0} is the yield stress at the neutral plane.

$$\sigma_{rz} = \sigma_{m0} \cdot \varepsilon_{rz}^{0.5} \tag{8}$$

$$\sigma_{ret} = \sigma_{m0} \cdot \varepsilon_{ret}^{0.5} \tag{9}$$

Based on the results obtained, a particular $Ra_0 \cdot h_0$ plane, which exists in different materials at different depths of sections h_0 and is called the neutral plane $K_{plmat0} = Ra_0 \cdot h_0$, was found and proved. It is always present in the section where the relatively smooth wall ends, and the periodic striations begin. By checking the statistics of many samples and materials, it has been found that this plane can be expressed as the ratio $h_0 = K_{plmat0}/Ra_0$, or as the ratio $h_0 = h_{lim}/Ra_0$, and the neutral plane is then given by the product $K_{plmat0} = Ra_0 \cdot h_0$. The change in tool parameters, the change in tool stiffness, the change in material cutting resistance, and the overall process dynamics then revolve around these neutral values in the actual process and the theoretical model. The expected result will be the derivation of stress–strain relationships as functions that use the knowledge of surface parameters and the construction of transformable stress–strain diagrams, partially according to the basic material groups (ferrous metals, steels, non-ferrous metals, polymers, elastomers, hard metals, technical ceramics, composite materials).

The neutral plane is theoretically defined as the reference plane. As a result of the equality of tensile and compressive stress $\sigma_{ret} = \sigma_{rz}$ (Fig. 2), it is valid that $Ra_0 = 3.7 = const$. This tensile-compressive stress equation is statistically verified for all materials, resulting in the relation (10) for the depth of cut in the neutral plane h_0.

$$h_0 = \frac{K_{plmat}}{Ra_0} = \frac{Ra \cdot h}{Ra_0 \cdot Y_{ret}} = \frac{K_{pl}}{Ra_0 \cdot Y_{ret}} \tag{10}$$

The deformation region at the level of the depth of cut in the neutral plane h_0 is given by relation (11).

$$K_{plo} = Ra \cdot h_0 \tag{11}$$

The expressions of the ratio of the introduced parameters K_{pl}/K_{plmat} or $1 + K_{pl}/K_{plmat}$ can be formulated terminologically most accurately as strengthening factors during material loading. Figure 2 shows the course of the total deformation stress σ_{sum} including its components, i.e. the compressive component σ_{rz} and the tensile component σ_{ret}; then the courses of the total surface roughness Ra_{sum} including the courses of its components, i.e. the compressive component Ra_{rz} and the tensile component Ra_{ret}, as well as the courses of the total value of Young's modulus of elasticity in tension including the courses of its components, i.e. the

compressive component E_{rz} and the tensile component E_{ret}. As part of the time development of the depth of cut $h(t)$, the h_{el} depth of cut is also shown, in which the compressive and tensile components of the surface roughness and h_{lim} as the limiting depth of cut are in equilibrium.

Since the other main surface deformation parameters are functionally interrelated, it will generally apply that $(Ra, \delta, Y_{ret}, h) = f(\sigma_{rz}, \sigma_{sum}, E_{rz}, E_{sum})$ in the compression region, and reciprocally for the same quantities in the tension region. The pressure components are increasing functions according to $h(t)$, and the tensile components are decreasing functions according to $h(t)$, intersecting at nodes A, B, and C on the neutral yield point plane h_0, or the elastic limit plane h_{el}. The geometric sum of the compressive and tensile components gives the basic shape of the distribution of roughness values and the relationship of the topographic function in the radial direction $Ra_d = f(h(t))$.

For the mathematical expression of the continuity/connectivity of the functions plotted in the modulus, stress, and strain regions in relation to the depth $h(t)$ in the plot in Fig. 3, the partial term in relations (4) and (5) below the square root is an important factor. This is the ratio of the deformation regions in the plane of the general and material divisibility constants $K_{pl}/K_{plmat} = Ra \cdot h/(Ra \cdot h/Y_{ret})$.

This ratio is also valid for the neutral plane: $K_{pl0}/K_{plmat} = Ra_0 \cdot h_0/(Ra_0 \cdot h_0/Y_{ret0}) = 1$, because $Y_{ret0} = 1$. In principle, it is a simple ratio of the product of the instantaneous roughness Ra and the instantaneous depth h in the general plane and the product of the roughness Ra_0 and the depth h_0 in the neutral plane, where $Y_{ret0} = 1$.

The notation according to relation (4) applies to pressure, and reciprocally, relation (5) applies to tension. The use of this relation allows the evaluation and plotting of continuous functions in dependence on $h(t)$ in both elastic and plastic stress–strain regions. This is because, from the classical elastic-rigidity point of view, the introduced ratios are a functional expression of the relative deformations in the sense of the generalised Hooke's law $\sigma_{rz} = E_{mat} \cdot \varepsilon_{rz}^n$. The
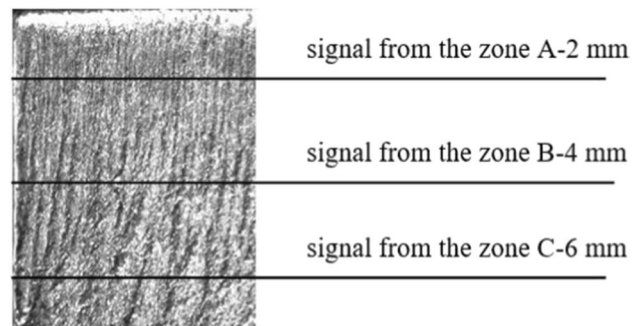

Fig. 3 The character of the walls made by abrasive water jet

signal from the zone A-2 mm

signal from the zone B-4 mm

signal from the zone C-6 mm

relations for compressive stresses in cut can be written in general in the forms (12).

$$\sigma_{rz} = \sqrt{E_{rz}} \qquad (12)$$

For the attenuation, dissipation component of the compressive stress, relation (13) subsequently applies:

$$\sigma_{rzx} = \sigma_{rz} \cdot cos\delta, \qquad (13)$$

where $cos\,\delta$ is the attenuation, dissipation factor in flexible tool cutting technologies. The deviation angle of the trace δ actually relieves the tension in the cut. For a sharp and rigid tool, such as an unblunted turning knife, where $\delta = 0$, cos $\delta = 1$, and $\sigma_{rzx} = \sigma_{rz}$.

2.3 Experimental procedures

The abrasive water jet cutting system CNC WJ2020B-1Z-D was used in the experiment. One hundred twenty samples with an examined area of 20×20 mm from AISI 1020 steel were machined using AWJ technology. The main cutting parameters used were as follows: pressure p of 300 MPa, nozzle diameter d_o of 0,25 mm, distance of the nozzle L from the surface was 2 mm, cutting speed v_p was 200 mm·min^{-1}. Recycled Garnet 80 MESH was used as an abrasive for abrasive water jet cutting. The grid projection method was used for the measurement of AISI 1020 steel samples. The appropriate measured and evaluated areas are demonstrated in Fig. 3.

Several methods of dealing with 3-D information obtained from camera images have been developed in recent years. The massive expansion in computer production technology creates new possibilities in developing rapid, fast, and precise exact techniques for treating digital image creation. The FRINGE program covers three measuring principles of the treatment of 3-D-elevated images: the method based on the projection grid, the method of a shift in phase, and the method of grey code.

The projection grid method (Fig. 4) of the projection grid allows us to define a relatively elevated position of individual points in the measured field from one that of the image set of the camera. The principle of the projection grid is so that if the investigated surface is of a uniform height built (i.e. the construction planes have regularly spaced distances), then the horizontal or inclined plane projects onto parallel lines, which are colour-distinguished. The unevenness of the surface with a line grid projection creates irregularities in the grid image projected by optics. The detected height 3D information is transferred into an image of a colour picture, which appears on the computer monitor. The colour image of the 3-D image can be interlaced with arbitrary profiling cuts for other geometrical analyses or separated into a 2-D profile.

3 Results and discussion

3.1 Analysis of the signals obtained by the grid projection method

Information about the structure of the surface is obtained from signals of the surface profile from zones A, B, and C. To better characterise and determine the stochastic and periodic components, in practice, the autocorrelation function of the complete topographical profile has been used to analyse signals. The classification of surface parameters through two components (the stochastic and the periodic ones) is proposed in [63]. The authors are motivated to draw this conclusion by the fact that the short-wave unevenness, especially roughness, is caused by the stochastic character of the disintegration induced by particular abrasive particles of the AWJ. On the other hand, they attribute rising

Fig. 4 The principal scheme of the grid projection method and overall view of the device
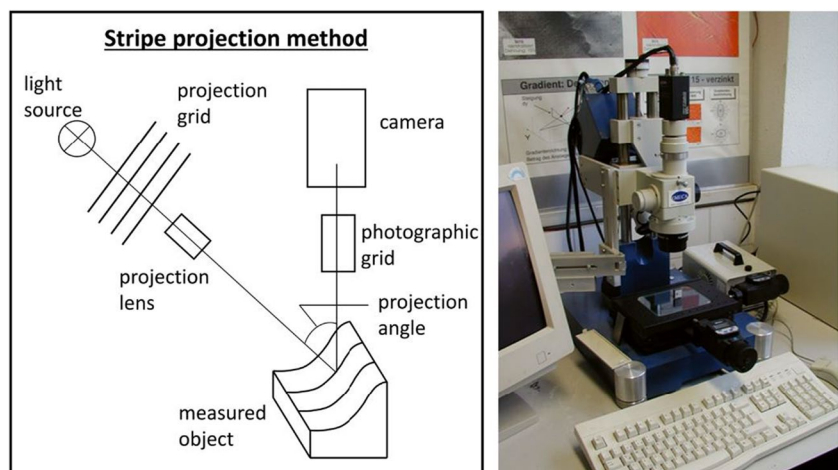
waviness to the periodical character of energy influences, with essentially lower frequencies affecting the disintegration process from outside (fluctuation of technological parameters of AWJ, vibrations of the machine and workpiece, etc.). The evaluation of the autocorrelation function provides the tool for mathematical manipulation with the topographic function of the geometrical form of the surface and enables us to find the so-called autocorrelation length and autocorrelation coefficient. The results convinced us that it is possible to detect and quantitatively determine both the stochastic as well as the periodic character of surface topography and thus quantify the statistics of the height fluctuations.

It can be seen major differences in the course of autocorrelation functions evaluated from the measured data on the surface created by AWJ. The experimental results obtained show that the surface correlation length increases along a trace of the abrasive water jet. The correlation length represents the horizontal property of a surface profile. The stochastic component in the upper part of the cut is much bigger than in the lower part. The results are expressed for AWJ in Figs. 5, 6, and 7, where the visible qualitative difference of the cutting zones to both the stochastic and the periodic zones is evident. The analysis of the autocorrelation function gives information about the autocorrelation length as a function of pitches of surface unevenness (it corresponds to the wavelength of surface topography).

The spectra obtained give information about the quasi-periodical as well as the random part; moreover, we can distinguish the amount of waviness and roughness (Fig. 8). From the practical point of view, the spatial frequency range can be divided into a spectrum composed of three parts, namely $(0–2.5)$ mm^{-1} — the waviness; $(2.5–20)$ mm^{-1} — grooving and slotting, which is hard to distinguish from
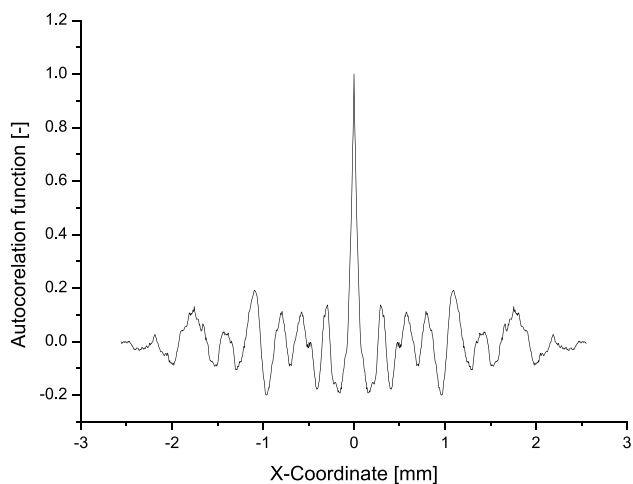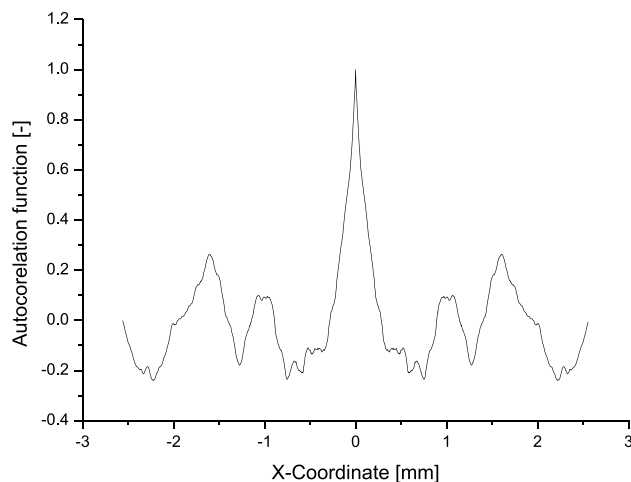
the roughness $(20–100)$ mm^{-1} because they depend on the vibration of water equipment.

It is believed that:

1) The waviness — is due to the instability of the abrasive water-jet, owing to outflow (discharge, flowing out) and consequently to fluctuation in the pressure pump;
2) In the spectrum, other components (defects) are superimposed, namely from lateral vibration and longitudinal vibration of the jet's mechanical equipment. By stopping the water jet, a dimple is created in the wall, and thus, the groove is extended;
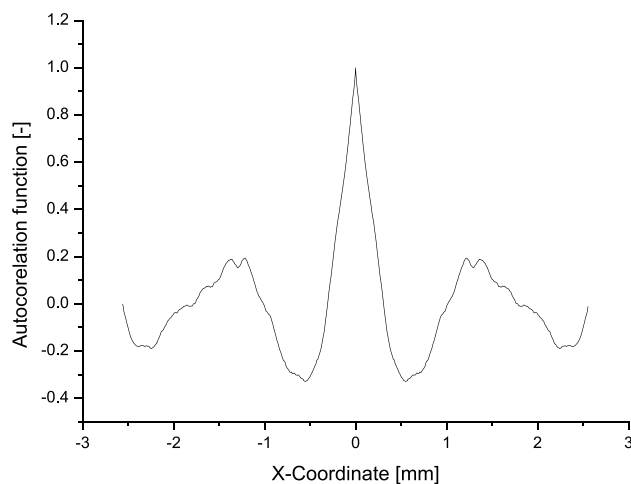3) Roughness — is due to random influences such as the cavitation effect, rising turbulence, etc.

Fig. 6 Autocorrelation function — zone B

Fig. 5 Autocorrelation function — zone A

Fig. 7 Autocorrelation function — zone C

Fig. 8 Frequency spectra of the surface signal-abrasive water jet

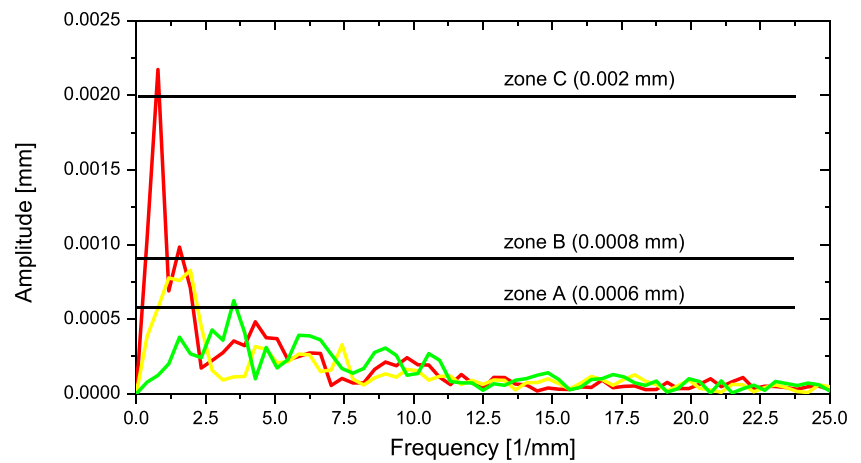**Table 1** The spatial frequency range divided into a spectrum

Order	Frequency	Wavelength
	$[1 \cdot mm^{-1}]$	[mm]
I	$f \leq 2.5$	$\lambda \geq 0.2$
II	$2.5 < f \leq 20$	$0.2 > \lambda \geq 0.05$
III	$f > 20$	$\lambda < 0.05$

A classification table with general validity has been created from these three areas. More than 5000 spectra were analysed to create the classification in Table 1.

The spatial frequency range can be divided into a spectrum composed of three parts:

    I.   Waviness,
   II.   Grooving-slotting,
  III. Roughness.

3.2 Method of determining the equivalent mechanical parameters of materials from the surface topography produced using a hydro-abrasive tool

According to the current state of the art, the elastic-strength or stress–strain mechanical parameters of the structural materials in question with the recording of the loading diagram σ-ε are determined on blast machines or on compression presses on small material samples precisely shaped and precisely loaded according to the current standards. Therefore, they are very laborious and lengthy procedures, both technically and financially demanding. However, the material parameters obtained in this way are only adequate for standard laboratory measurement conditions, as they are mainly related to artificial uniaxial stresses and do not take into account the actual operating dimensions of the components and conditions, nor do they cover the combinations

of different types of stresses commonly encountered in engineering practice. At the same time, the stress–strain behaviour of the material in the elastic–plastic and plastic transformation region cannot yet be predicted quantitatively and graphically with sufficient accuracy, either on the basis of these measurements or theoretically for design purposes. The transformation character of each material is of fundamental importance for the designer and must also be expressed as accurately as possible by the σ-ε load diagram and the tabulated material values. However, the current laboratory tests are based (due to the still problematic solution of the elastic–plastic and plastic transformation region) not on the actual but on the so-called contractual parameters of the σ-ε diagram, and these are subsequently also given in the material tables.

The presented method of determining the equivalents of mechanical parameters of materials from the surface topography created by a flexible cutting tool eliminates the disadvantages by enabling the identification of stress–strain mechanical equivalents of mechanical parameters of materials from the analysis of surface roughness and from their change in specific functional conditions in a more comprehensive way and with disproportionately lower labour, material–technical, and financial requirements. The course of stress–strain behaviour of the material in the elastic–plastic and plastic transformation region can be not only quantitatively and graphically determined but also predicted based on the proposed method for the needs of design and engineering practice, i.e. mathematically modelled technical prediction for the assumed types of functional stress, corrosion intensity, etc. According to this method, it is also possible to predict and determine the equivalents of elastic-strength parameters with higher strength than the strength of the abrasive material (for garnet $R_m = 3\,500$ MPa). The abrasive strength significantly limits the use of AWJ technology, in particular, based on the results obtained from the basic material composition. The numerical values, graphical

outputs, and loading diagrams σ-ε or F-ΔL, according to the new method of determination, complement the laboratory data and express more comprehensively the actual characteristics of each structural material. Surface analysis methods are described in the world literature, but not in terms of their use for evaluating the stress–strain behaviour of the material but only in terms of describing the geometry of the material surface.

In order to verify the method, hundreds of materials most commonly used in industrial practice were measured and calculated, with the possibility of documentation, ranging from very soft and plastic to very strong, flexible, hard, and brittle metallic structural and building materials, rocks, and plastics, i.e. materials with a very good agreement ($\pm 5\%$) with the tabulated values declared in the literature.

The essence of the solution is to use the geometric parameters of the cutting path after the action of the flexible cutting tool. The cutting tool responds accurately and measurably to the instantaneous resistance of the material so that the material constant K_{plmat} [mm] can be determined by measuring the surface roughness Ra [μm] of the cutting path at any measured depth h [mm] according to relation (14). Subsequently, the desired equivalent of Young's modulus of elasticity E_{mat} can be determined according to relation (15).

$$K_{plmat} = \frac{10 \cdot h_x}{Ra_x + h_x} = \frac{Ra \cdot h}{Y_{ret}} = \frac{10^{12}}{E_{mat}^2} \quad (14)$$

$$E_{mat} = \left(\frac{Ra_x \cdot 10^{11}}{0.1 \cdot Ra_x \cdot h_x + h_x} \right)^{0.5} \quad (15)$$

From the parameter K_{plmat}, it is possible to determine the equivalents of the mechanical parameters of the materials, from the topography of the surface created by the flexible cutting tool in both the elastic and the plastic region of the reshaping, including numerical and graphical parameters for technical and actual σ-ε and F-ΔL diagrams, including the determination of the reshaping limits, as well as actual and technical σ-ε and F-ΔL diagrams at the specified deformation limits for materials with above-limit strength.

In accordance with the above solution of the problem, the construction of the σ-ε diagram is shown in Fig. 9, from the values of the static equivalents at each strain transformation limit. In particular, it is the elastic limit true/engineering M_{el}, the yield limit true/engineering M_{kl}, than the elastic–plastic limit true/engineering M_{ppl}, the ultimate tensile strength true/engineering M_{rm}, the plastic limit true/engineering M_{creep}, and the strength limit true/engineering M_{pt}.
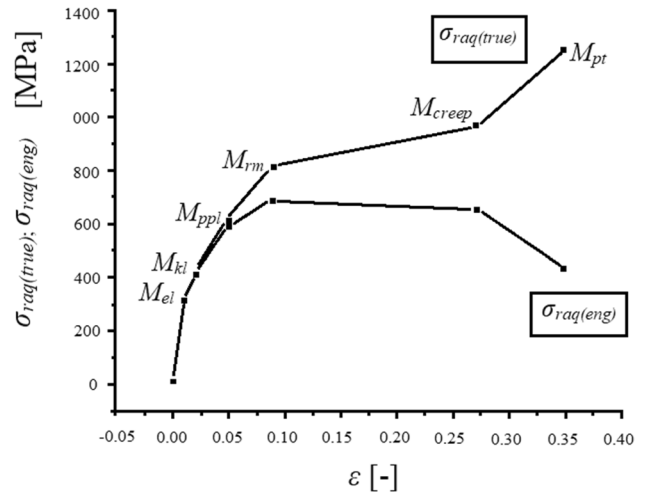

Fig. 9 Construction of the σ-ε diagram from the values of the static equivalents on the individual deformation limits of the transformation

3.3 Conversion to σ-h_def and σ-ε diagrams according to the cut wall roughness

It is possible to build on the above analytical basis for the conversion to the tensile strain dependence σ-h_{def} or σ-h_{cut} and, at the same time, to use the radial roughness Ra_q measured across the paths, i.e. in the radial plane of the flexible cut, instead of the path roughness Ra. Indeed, this introduction allows identifying the position of the yield point at a depth of section h_{cut} very precisely, including identifying the details of the upper $Re(up)$ and lower $Re(d)$ yield point. For radial roughness Ra_q, the Eq. (16) is valid:

$$Ra_q = Ra_0 \cdot \left(log\ h^2 + log(h \cdot tg\delta)^{-0.25} \right)^{\frac{2}{3}} \quad (16)$$

From here, the relation for refining the strain stress distribution (17) can be easily obtained,

$$\sigma_{raq} = 10^3 \cdot \frac{E_{mat} \cdot Ra_q}{Ra_0} \quad (17)$$

as well as the relation for the relative deformation (18).

$$\varepsilon_q = \frac{\sigma_{raq}}{E_{mat}} \quad (18)$$

Therefore, it is the case of an application of the general Hooke's law according to relation (19):

$$\sigma_{raq} = \varepsilon_q \cdot E_{mat} \quad (19)$$

For the steel AISI 1020, the graph of the working diagram is shown in Fig. 8. The details of the diagram σ_{raq}-h_{def} can be commented as follows. The values on the neutral plane,

i.e. on the plane at the level of the neutral strain length h_0 are as follows: $Ra_{q0} = (9.1581 + 1.3168i)$, $Ra_0 = 3.7$, $Y_{ret0} = 1$, $\delta_o = 8.58°$.

The value of radial roughness is calculated by adding the values on the neutral plane (20), coming out as a complex number.

$$Ra_{q0} = Ra_0 \cdot \left(log \; h_0^2 + log\left(h_0 \cdot tg\delta_0\right)^{-0.25} \right)^{\frac{2}{3}} \qquad (20)$$

Stress in the technical branch is $\sigma_{raqo} = Re = 270$ MPa (Table 2). Then, $\sigma_{raqo(\text{actual})}$ is 291 MPa in the actual stress branch. The stress difference between the upper and lower yield point is quite high and is 21 MPa. It is due to the boundary shear at the transition from tension to compression, namely in the evolution of the character of the induced stress in the material σ_{ret}/σ_{rz} (Fig. 2).

3.4 Analytical calculation and construction of the σ_{raq}-h_{def} diagram

The original starting point for deriving the principal relations was the cuts generated by the flexible hydro-abrasion AWJ tool, from which the diagram σ_{raq}-h_{def} was evaluated. The parameter h_{def} actually represents the depth of cut h_{cut} (mm) and within this depth of cut are significant points, i.e. the depth of cut h_{el}, in which the compressive and tensile component of the surface roughness R_{el} are in equilibrium. The depth of cut h_{re} corresponds to the

yield point Re and the depth of cut h_{rm} corresponds to the tensile strength Rm.

The graph in Fig. 10 describes the construction and significance of the intersection of the tension and compression branches of σ_{ret}/σ_{rz} to identify the position of the neutral plane at depth level h_0 and the upper/lower yield point $Re_{(up)}/Re_{(d)}$, as well as the overall distribution of $\sigma_{raq(\text{actual})}/\sigma_{raq(\text{eng})}$ in the diagram σ_{raq}-h_{def} and the position of the strain limits. The h_{iz} symbol represents the range of the so-called initiation zone of the tool penetration into the material. The initiation zone h_{iz} is characterised by higher roughness and higher material resistance to the tool at nanometric surface depths. In particular, Fig. 10 identifies the stress values at the main limits and in detail, the evolution of the true and engineering stresses in the regions of the upper and lower yield point and the initiation zone h_{iz}, as well as the range and value of the tensile stress component σ_{ret} in the residual deformation depth region h_{lim}-h_{crit}.

The graph in Fig. 11 shows a detail of the internal friction angle $\delta = f(h_{def})$, including the expansion frequency in the area of the depth of residual deformation h_{lim}-h_{crit} as the difference between the depth of limit deformation h_{lim} and the critical depth h_{crit}. An important parameter is the break depth h_{break}, which is located between the depth corresponding to the tensile strength h_{rm} and the depth critical h_{crit}. The amplitude frequency δ characterises the frequency of mechanical vibration.

3.5 Analytical calculation and construction of the σ_{raq} - ε diagram

The theoretical basis of the solution, according to subsection 2.3, is also fully valid in the case of the calculation and construction of the transformation diagrams σ-ε. In general, and simplified terms, the relative elongation in the radial deformation plane can be expressed by the ratio

Table 2 Mechanical parameters of AISI 1020 steel, where Z is the contraction

E_{mat} [MPa]	Re [MPa]	Rm [MPa]	A [%]	Z [-]
201 200	270	343	15	0.4

Fig. 10 Detail of the evolution of the actual and technical stresses in the regions of the upper and lower yield strength and the initiation zone h_{iz}
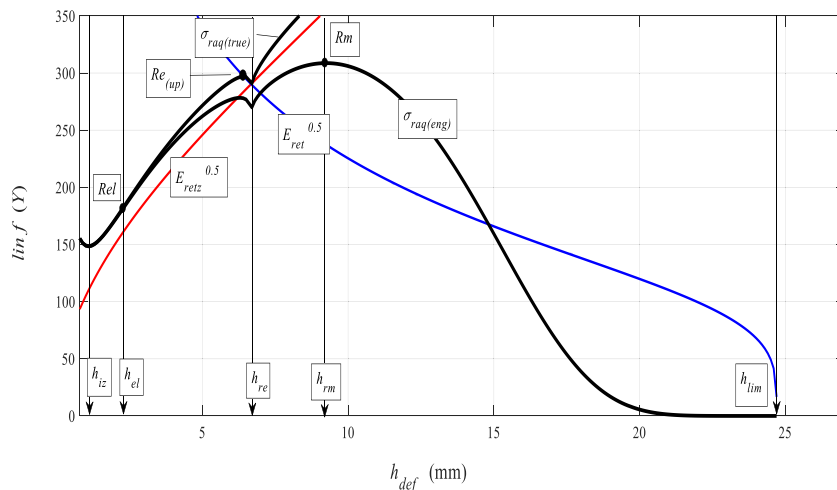
Fig. 11 Detail of the internal
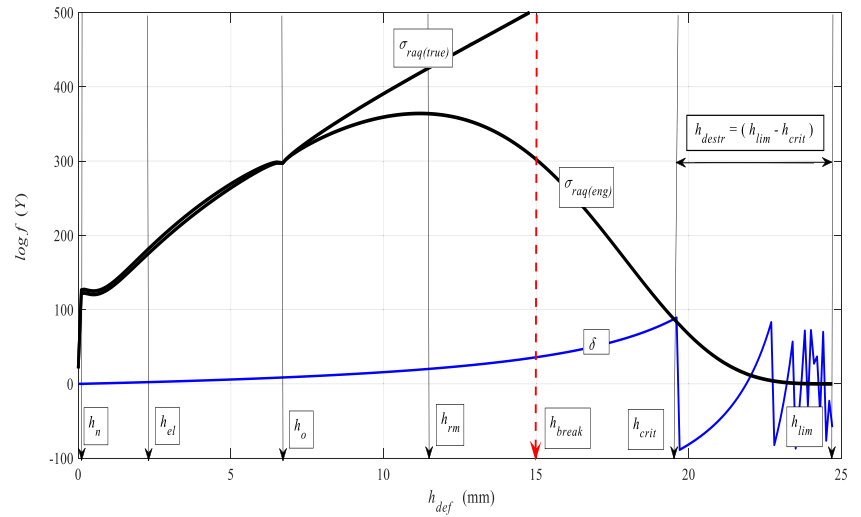friction angle $\delta = f(h_{def})$

Fig. 12 Detail of the evolution of the actual and technical stresses in the upper and lower yield strength regions for AISI 1020
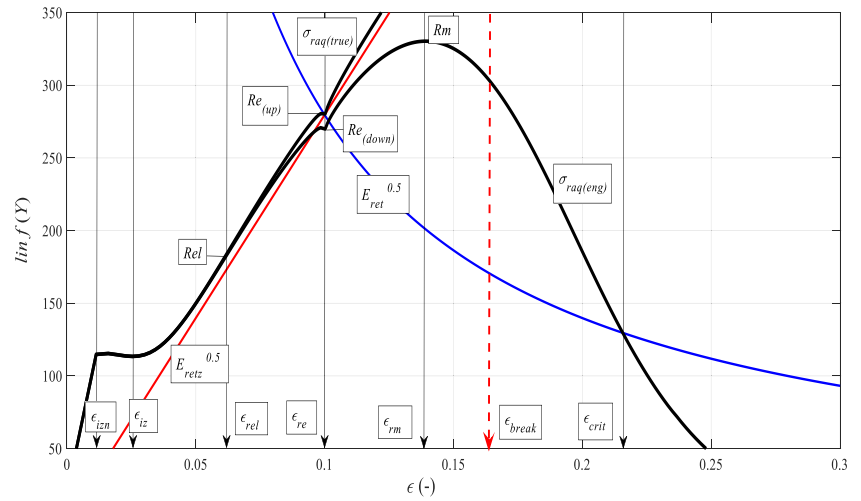

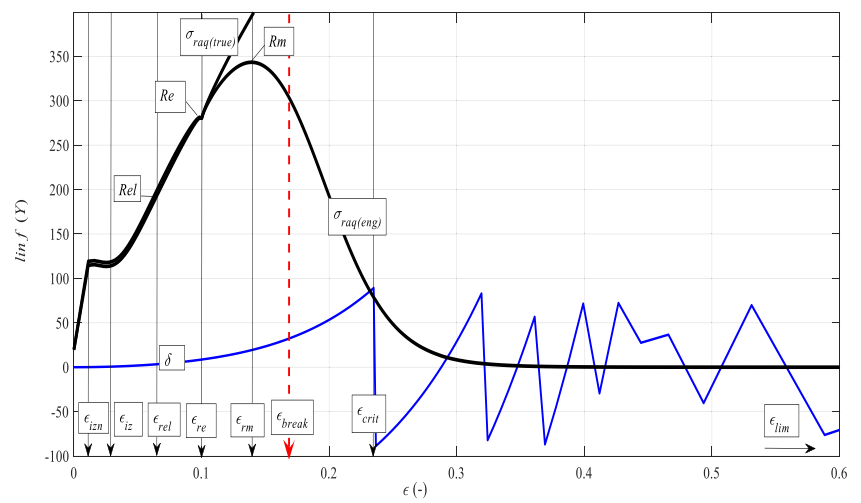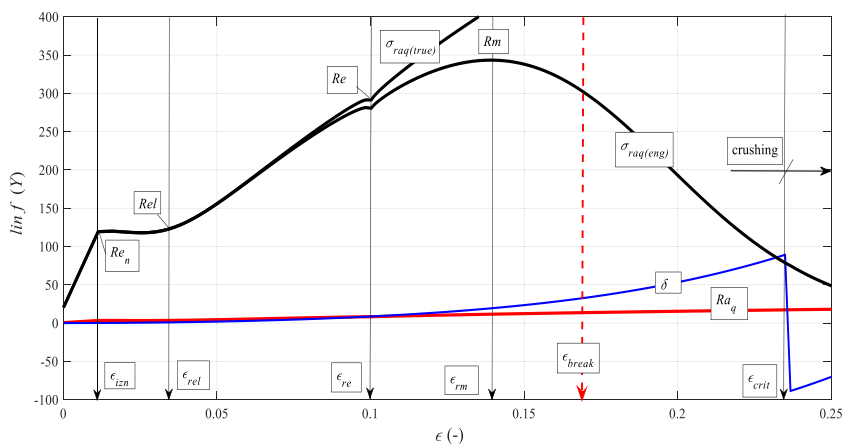**Fig. 13** Overall evolution of the real and technical stress for AISI 1020

Fig. 14 Analytically predicted stress–strain parameters at technically important limits

$\varepsilon_q = \sigma_{raq}/E_{mat}$ according to relation (18). Then, the ductility is expressed as $A = 100 \cdot \varepsilon_q$ [%]. The conversion of $\varepsilon_q = f(h_{def})$ can be done using the coefficient $K_{h\varepsilon} = f(h_{cut})$, according to the ratio on the neutral deformation plane $K_{h\varepsilon} = K_{h\varepsilon0} = \varepsilon/h_{q00}$. Then, it follows $\varepsilon_q = K \cdot h_{h\varepsilon def}$. The function $\cos \delta$ represents the attenuation factor.

The graphs in Figs. 12, 13, and 14 are constructed analogously for the case of dependence on the deformation depth h_{def}. In cases depending on the relative deformation $\sigma_{raq} = f(\varepsilon_q)$, a graphical highlight of the initiation zone of the relative elongation ε_{iz} in the initiation zone can be seen. Other important points are the relative elongation for the elastic limit ε_{re}, the relative elongation ε_{rm} at the ultimate strength, the relative elongation corresponding to material failure ε_{break}, and the critical relative elongation ε_{crit} corresponding to the limit depth.

Figure 14 shows an example of a method of prediction of stress deformation parameters at technically important limits, both in terms of AWJ technology requirements and in terms of design dimensioning. The values of the parameters at the individual limits are given by calculation or result from the graphs according to the proposed methodology. The break limit ε_{break} is newly added, which is a function of the break depth h_{break} (mm), the ratio $K_{h\varepsilon} = \varepsilon_0/h_0$ (-), and the roughness on the neutral plane $Ra_0 = 3.7$ (µm) according to the newly proposed, experimentally derived logarithmic Eq. (21).

$$\varepsilon_{break} = e^{ln(h_{break} \cdot K_{h\varepsilon} \cdot Ra_0)} \tag{21}$$

where:

$$h_{break} = h_{breakj} \cdot ln\left(\frac{Re}{K_{plmat}} - 1\right) \tag{22}$$

where h_{breakj} is unit of break depth.

3.6 Mechanism of formation of surface topography created by hydroabrasive cutting

Let the force acting on the beam create a deflection, which is numerically reflected in the deformation of this beam. By analogy, if we consider the pressure from the pump, which is 300 MPa in our case, it also causes a deformation that is reflected in the surface topography in the form of changes in geometric parameters, namely the surface roughness Ra and the delay of the ray trace Y_{ret} during the hydroabrasive splitting of the material [64, 65]. These geometrical parameters can be considered as deformations, in which the information is encoded about the formation of the surface layer, which is the memory of the technology, in our case, of hydroabrasive cutting. For the calculation of this area S, we assume that the diameter of the abrasive water jet, according to Hashish, is $r = 0.8$ mm. Then, the area can be expressed according to relation (23):

$$S = 4\pi \left(\frac{0,8}{2}\right)^2 \tag{23}$$

Based on the calculated area S, we can determine the maximum force that could be generated at a given contact area (24). Thus, this force is:

$$F = p.S = 600N \tag{24}$$

Based on the analysis of the amplitude-frequency spectra and interpretation of the measured data by the grid projection method, and comparison of these data with the data obtained by the FRT optical profilometer and the HOMMEL TESTER T800 contact profilometer, we proposed criterion C according to (2) in [66] based on which we try to determine the percentage of waviness to roughness in a given horizontal measurement line. However, this proposed parameter has the disadvantage

that we cannot use it in general but only specifically for measurements at given settings of illumination angle, light parameters, etc. Therefore, we introduce the parameter P, which has general validity and, in addition, is related to the material to be machined through the relative longitudinal elongation. For this parameter, the main point is that, based on the analysis of amplitude–frequency spectra, there is a desire to seek a link between the optically measured data in relation to the material because it is undoubtedly necessary to reflect on the current lack in the world when the material characteristics are not sufficiently respected, and the surface roughness is considered only as a geometric change; but if we imagine a beam that we load, we can observe that it is cratered, which increases the surface roughness. This parameter P is mainly based on the idea that the surface layer encodes information about the technological parameters and the way the material is loaded and, therefore, formed by the concerned technology. The ratio $\frac{RMS_s(1)}{RMS_s(-RMS_s(1))}$ can be thought of as the deflections in the individual levels when related to depth. This ratio will increase with depth and therefore, the deflections will also increase; these deflections can be seen simply as the surface roughness Ra, since the RMS_s is directly related to Ra. Thus, for us, Ra is a deformation that varies with depth according to the corresponding load. This load is characterised by the loading force, and it is possible to use this parameter to go on to calculate the forces required to produce Ra, Y_{ret}, and h. Therefore, we need to introduce the appropriate surfaces on which the loading force acts.

$$P = \left(\frac{RMS_s(1)}{RMS_s\left(-RMS_s(1)\right)} \right) \cdot \varepsilon \tag{25}$$

where ε is the relative longitudinal elongation for the material, which is calculated as follows (26):

$$\varepsilon = \frac{\sigma}{E} = \frac{p}{E} \tag{26}$$

The instantaneous increments of the abrasive-contact surfaces can be expressed as multiples of the instantaneous increments of the deformations in the corresponding planes according to (27) and (29).

$$S_{xzi} = Ra_i \cdot h_i = S_{Rahi}, \tag{27}$$

$$S_{xyi} = Ra_i \cdot Y_{reti} = S_{Rayi}, \tag{28}$$

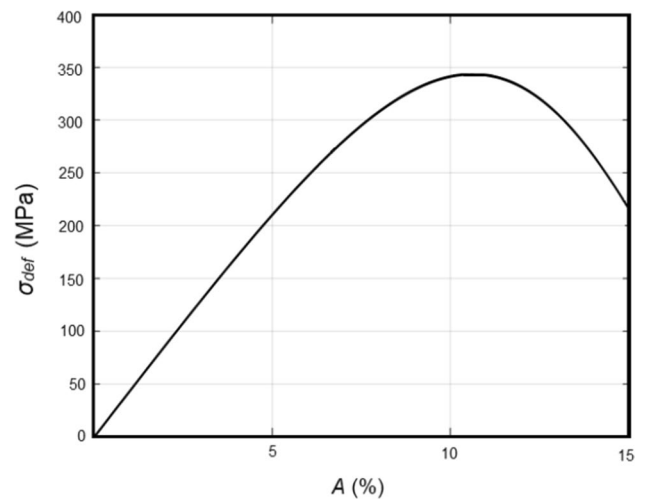$$S_{yhi} = Y_{reti} \cdot h_i = S_{yhi}, \tag{29}$$

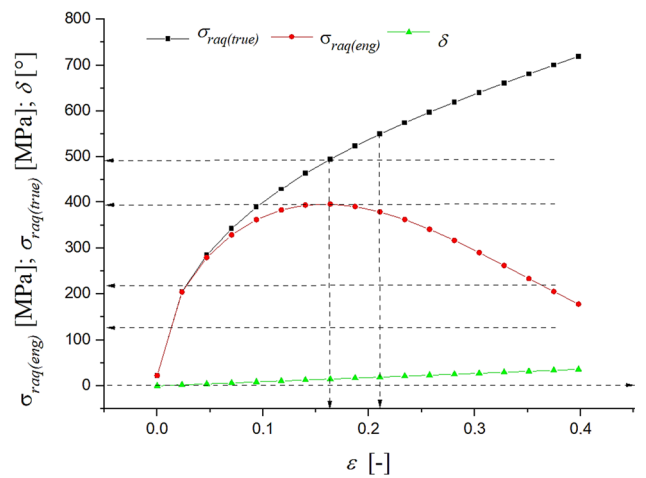**Fig. 15** Construction of the σ-A curve from the real data

Fig. 16 Construction of the σ-ε curve from the calculated data

The total force is then expressed as:

$$F = \sqrt{\left(S_{Ra_i \cdot h_i}\right)^2 + \left(S_{Ra_i \cdot Y_{\mathrm{reti}}}\right)^2 + \left(S_{Y_{\mathrm{reti}} \cdot hi}\right)^2} \tag{30}$$

The experimental results were continuously compared with the theory, and a mutual agreement was established, even when using the extensive statistics that the authors already had available [65, 66].

3.7 Comparison and verification of the model

The laboratory measurement of the σ-A diagram was carried out according to the standard in the accredited laboratory of the VÚHŽ Dobrá Research Institute in the Czech Republic.

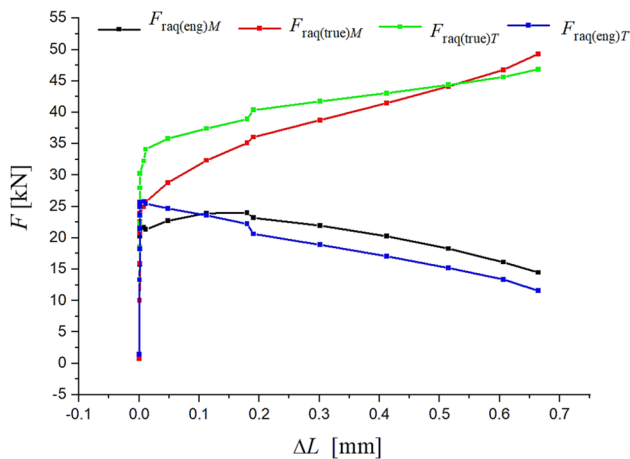**Fig. 17** Dependence of force F on absolute elongation ΔL, comparison of measured M and theoretical T values

Stress measurements were performed with an accuracy of 0.1 MPa and ductility measurements with a precision of 0.001%. According to the data, the shape of the deformation diagram of AISI 1020 steel is shown in Fig. 15.

In Fig. 16, a diagram of the dependence of the engineering stress $\sigma_{raq(eng)}$ and the true stress $\sigma_{raq(true)}$ on the proportional elongation ε is created for AISI 1020 steel, and in Fig. 17, the actual measured M and calculated theoretical T forces are plotted for comparison, while the difference between them is up to 10%.

3.8 Application and significance of the method for determining the mechanical parameter equivalents of materials from surface topography produced by a flexible cutting tool

In particular, the new derivation method can be used to evaluate:

- Physical relations for material parameters and transformation parameters,
- Equilibrium stress–strain functions of surface topography,
- Deformation capacity, plasticity coefficient K_{plmat}, and their relation to E_{mat},
- Relationships between surface topography parameters in the cutting path and in the radial plane,
- Method of solving stress–strain functions according to surface topography,
- Partial effect of tensile and compressive stress components on surface deformation,
- Topographic surface features,
- Method of calculating mechanical parameter equivalents from surface topography,

- Method of constructing the equivalent diagrams $\sigma\text{-}h_{cut}$, $\sigma\text{-}h_{def}$, and $\sigma\text{-}\varepsilon$ from the cut parameters.

The method of determining the mechanical parameter equivalents of materials from surface topography produced by a flexible cutting tool allows simple, inexpensive, express, and accurate determination of mechanical parameter equivalents of materials in a non-contact, non-destructive manner, and also allows a simple operational check of mechanical parameters in an express manner.

This method can also be applied to the measurement of topographies of surfaces created by various technologies with flexible cutting tools, such as not only hydro-abrasive cutting but also laser, plasma, and oxygen, i.e. the mechanical constant of the material K_{plmat} can be determined according to the measured geometric parameters of the cutting path, and the positions of the transformation limits and equivalents of the mechanical parameters of various technical materials machined by various technologies can be determined by analogy.

The proposed solution can be used in all companies, plants, and research institutes dealing with the separation of technical materials. The database of measured equivalents can be tabulated for individual so-called pure materials as well as for whole groups of metabolically related materials and alloys. Advantageous use can be expected in workplaces dealing with the determination of mechanical parameters and transformation properties of technical materials, design and construction calculations, mathematical modelling of the stability of buildings and structures, and the development of new materials with the required mechanical properties.

4 Conclusions

The presented paper mainly deals with the solution of geometric parameters of the topography of surfaces generated by the technology of flexible hydro-abrasive cutting. Based on the analysis and interpretation of the obtained surface data, a topographic function is derived in an original way, which is the basis for further analysis as well as for the prediction of the quality of the hydro-abrasive cutting technology. The mathematical principles governing the constraints are newly formulated.

In the interpretation of the measured values, the relationships between topographic, technological, and physical–mechanical parameters of the material are systematically analysed. The basic relations for the prediction calculation of the roughness of the cut walls are presented, as well as other relations derived by modification of these basic relations for the identification of mechanical parameters and the reshaping, up to the analytical construction of the reshaping diagrams of the cut materials.

Flexible hydro-abrasive tools are the most suitable for study because they are characterised by a flexible and identical response to resistance in the tool-material contact in the cutting path. The roughness of the cutting surface is relatively easy, accurate, and quick to measure. It responds identically to instantaneous fluctuations in tension/pressure ratios throughout the depth of cut. The change in the distribution of roughness at the depth limits is often stepwise, especially for harder materials, and can be observed with a microscope, magnifying glass, or even the naked eye. The roughness can be easily converted to strength and deformability parameters according to the newly derived relations, up to the calculation and construction of the reshaping diagrams. In this way, laboratory data will be supplemented, especially for the purpose of dimensioning mechanical and civil engineering structures, as well as for use in various precision engineering applications.

The way the issue has been dealt with can be summarised in the following main points:

1. A classification table of surface distribution after AWJ cutting with general validity was created. More than 5000 spectra from three areas have been analysed (I. waviness, II. grooving-slotting, III. roughness).
2. The method of determining the equivalents of mechanical parameters of materials from the surface topography of the formed flexible cutting tool is characterised by the fact that the mechanical constant K_{plmat} is subsequently determined on the basis of the measurement of the roughness Ra of the cutting path at any measured depth h.
3. The method of determining the equivalents of mechanical parameters is characterised by the fact that from the determined mechanical constant K_{plmat}, the tabular equivalents of mechanical parameters of materials in both elastic and plastic regions of transformation are determined, including numerical and graphical parameters for technical σ-ε and F-ΔL diagrams and/or for real σ-ε and F-ΔL diagrams, and/or for technical σ-ε and F-ΔL diagrams at the specified transformation limits, and/or for actual σ-ε and F-ΔL diagrams at the specified transformation limits, and/or for both actual and technical σ-ε and F-ΔL diagrams at the specified deformation limits for materials with above-limit strength based on the observed results from the basic material composition.
4. The method of determining the equivalents of mechanical parameters is characterised by the prediction of elastic-strength equivalents in both elastic and plastic regions of the transformation from the mechanical constant K_{plmat}, including numerical and graphical parameters of the actual and technical σ-ε and F-ΔL diagrams at the specified deformation limits for materials with above-limit strength based on the results obtained from the basic material composition.
5. The new method of prediction of stress deformation parameters at technically important limits, both in terms of AWJ technology requirements and in terms of design dimensioning, is presented.

Data availability All data and materials used to produce the results in this article can be obtained upon request from the corresponding authors.

Declarations

Ethics approval The authors declare that there is no ethical issue applied to this article.

Consent to participate The authors declare that all authors have read and approved to submit this manuscript to IJAMT.

Consent for publication The authors declare that all authors agree to sign the transfer of copyright for the publisher to publish this article upon on acceptance.

Competing interests The authors declare no competing interests.

References

1. Jain VK (2022) Advanced machining science. CRC Press

2. Gupta K, Gupta MK (2018) Developments in nonconventional machining for sustainable production: a state-of-the-art review. Proc. Inst. Mech. Eng. Part C: J Mech Eng Sci 233:4213–4232. https://doi.org/10.1177/0954406218811982

3. Kuttan AA, Rajesh R, Dev Anand M (2021) Abrasive water jet machining techniques and parameters: a state of the art, open issue challenges and research directions. J Brazilian Soc Mech Sci Eng 43(4):1–14. https://doi.org/10.1007/s40430-021-02898-6

4. Jankovic P, Igic T, Radovanovic M, Turnic D, Zivkovic S (2019) Applications of the abrasive water jet technique in civil engineering. Facta univ. - ser.: Archit. Civ Eng 17:417–428. https://doi.org/10.2298/fuace190710026j

5. Averin E (2017) Universal method for the prediction of abrasive waterjet performance in mining. Engineering 3:888–891. https://doi.org/10.1016/j.eng.2017.12.004

6. Nyaboro J, Ahmed M, El-Hofy H, El-Hofy M (2021) Experimental and numerical investigation of the abrasive waterjet machining of aluminum-7075-T6 for aerospace applications. Adv Manuf 9:286–303. https://doi.org/10.1007/s40436-020-00338-7

7. Kmeč J, Hreha P, Hlaváček P, Zeleňák M, Harničárová M, Kuběna V, Knapčíková L, Mačej T, Duspara M, Cumin J (2010) Disposal of discarded munitions by liquid stream. Teh vjesn 17:383–388

8. McGeough JA (2016) Cutting of food products by ice-particles in a water-jet. Procedia CIRP 42:863–865. https://doi.org/10.1016/j.procir.2016.03.009

9. Xiong S, Jia X, Wu S, Li F, Ma M, Wang X (2021) Parameter optimization and effect analysis of Low-Pressure Abrasive Water Jet (LPAWJ) for paint removal of remanufacturing cleaning. Sustainability 13(5):2900. https://doi.org/10.3390/su13052900

10. Hreha P, Hloch S, Magurová D, Valicek J, Kozak D, Harnicarova M, Rakin M (2010) Water jet technology used in medicine. Teh vjesn 17:237–240

11 Jagadish GK (2020) Abrasive water jet machining of engineering materials. Springer Cham, Switzerland

12. Martinec P, Foldyna J, Sitek L, Ščučka J, Vašek J (2002) Abrasives for AWJ cutting. Institute of Geonics Academy of Sciences of the Czech Republic, Ostrava, Czech Republic

13. Sarkar M, Jain VK (2017) Nanofinishing of freeform surfaces using abrasive flow finishing process. Proc. Inst. Mech Eng Pt B J Eng Manufact 231:1501–1515. https://doi.org/10.1177/0954405415599913

14. Sankar MR, Jain VK, Ramkumar J, Kar KK (2010) Rheological characterisation and performance evaluation of a new medium developed for abrasive flow finishing. Int J Precis Technol 1:302–313. https://doi.org/10.1504/IJPTECH.2010.031659

15. Sarkar M, Jain VK, Sidpara A (2019) On the flexible abrasive tool for nanofinishing of complex surfaces. J Adv Manuf Syst 18:157–166. https://doi.org/10.1142/S0219686719500082

16. Singh S, Raj ASA, Sankar MR, Jain VK (2016) Finishing force analysis and simulation of nano surface roughness in abrasive flow finishing process using medium rheological properties. Int J Adv Manuf Technol 85:2163–2178. https://doi.org/10.1007/s00170-015-8333-2

17. Jain VK, Adsul SG (2002) Experimental investigations into abrasive flow machining. Int J Mach Tool Manuf 40:1003–1021. https://doi.org/10.1016/S0890-6955(99)00114-5

18. Bitter JGA (1963) A study of erosion phenomena part I. Wear 6:5–21. https://doi.org/10.1016/0043-1648(63)90003-6

19. Bitter JGA (1963) A study of erosion phenomena: Part II. Wear 6:169–190

20. Hashish M (1988) Visualization of the abrasive-waterjet cutting process. Exp Mech 28:159–169. https://doi.org/10.1007/bf02317567

21. Hashish M (1984) A modeling study of metal cutting with abrasive waterjets. J Eng Mater Technol 106:88–100. https://doi.org/10.1115/1.3225682

22. Hashish M (1993) A modeling study of jet cutting surface finish. ASME-PUBLICATIONS-PED 58:151–151

23. Hashish M (1989) An investigation of milling with abrasive-waterjets. J Eng Ind 111:158–166. https://doi.org/10.1115/1.3188745

24. Shao Y, Cheng K (2019) Integrated modelling and analysis of micro-cutting mechanics with the precision surface generation in abrasive flow machining. Int J Adv Manuf Tech 105:4571–4583. https://doi.org/10.1007/s00170-019-03595-4

25. Marušić V, Baralić J, Nedić B, Rosandić Ž (2013) Effect of machining parameters on jet lagging in abrasive water jet cutting. Teh vjesn 20:677–682

26. Llanto JM, Tolouei-Rad M, Vafadar A, Aamir M (2021) Recent progress trend on abrasive waterjet cutting of metallic materials: a review. Appl Sci 11:3344. https://doi.org/10.3390/app11083344

27. Hassan A I,Kosmol J, Bursa J (2000) Analysis of stresses in abrasive waterjet machining (AWJM). In Proceedings of the Proceedings of the Conference: VI Konferencja Naukowo-Techniczny EC (Electromachining), Bydgoszcz, Poland, pp 24–25

28. Wu Y, Zhang S, Wang S, Yang F, Tao H (2014) Method of obtaining accurate jet lag information in abrasive water-jet machining process. Int J Adv Manuf Technol 76:1827–1835. https://doi.org/10.1007/s00170-014-6404-4

29. Orbanic H, Junkar M (2008) Analysis of striation formation mechanism in abrasive water jet cutting. Wear 265:821–830. https://doi.org/10.1016/j.wear.2008.01.018

30. Balamurugan K, Uthayakumar M, Gowthaman S, Pandurangan R (2018) A study on the compressive residual stress due to waterjet cavitation peening. Eng Fail Anal 92:268–277. https://doi.org/10.1016/j.engfailanal.2018.05.012

31. Dong X (2011) Surface mechanical characteristics and fatigue life experiments of premixed water jet peening strengthening. J Mech Eng 47:164. https://doi.org/10.3901/jme.2011.14.164

32. Hassan AI, Kosmol J (2001) Dynamic elastic–plastic analysis of 3D deformation in abrasive waterjet machining. J Mater Process Technol 113:337–341. https://doi.org/10.1016/s0924-0136(01)00687-2

33. Hashish M (1995) Material properties in abrasive-waterjet machining. J Eng Ind 117:578–583. https://doi.org/10.1115/1.2803536

34. Hashish M (1993) Prediction models for AWJ machining operations. Prediction Models for AWJ Machining Operations, 7th American Water Jet Conference, (Seattle, WA), p 205–216

35. Hashish M (1989) Pressure effects in abrasive-waterjet (AWJ) machining. J Eng Mater Technol 111:221–228. https://doi.org/10.1115/1.3226458

36. Hashish M (1993) The effect of beam angle in abrasive-waterjet machining. J Eng Ind 115:51–56. https://doi.org/10.1115/1.2901638

37. Perec A (2021) Research into the disintegration of abrasive materials in the abrasive water jet machining process. Materials 14:3940. https://doi.org/10.3390/ma14143940

38. Nguyen T, Wang J (2019) A review on the erosion mechanisms in abrasive waterjet micromachining of brittle materials. Int J Extreme Manuf 1:012006. https://doi.org/10.1088/2631-7990/ab1028

39. Hassan AI, Chen C, Kovacevic R (2004) On-line monitoring of depth of cut in AWJ cutting. Int J Mach Tools Manuf 44:595–605. https://doi.org/10.1016/j.ijmachtools.2003.12.002

40. Guo N, Louis H, Meier G (1993) Surface structure and kerf geometry in abrasive waterjet cutting: formation and optimization. Surface structure and kerf geometry in abrasive waterjet cutting: formation and optimization, 7th American Waterjet Conference, Seattle, Washington, USA, pp 1–25

41. Guo Z, Ramulu M, Jenkins MG (2000) Analysis of the waterjet contact/impact on target material. Opt Lasers Eng 33:121–139. https://doi.org/10.1016/s0143-8166(00)00027-0

42. Natarajan Y, Murugesan PK, Mohan M, Khan SALA (2020) Abrasive water jet machining process: a state of art of review. J Manuf Process 49:271–322. https://doi.org/10.1016/j.jmapro.2019.11.030

43. Thamizhvalavan P, Yuvaraj N, Arivazhagan S (2021) Abrasive water jet machining of Al6063/B4C/ZrSiO4 hybrid composites: a study of machinability and surface characterization analysis. SILICON 14:1093–1121. https://doi.org/10.1007/s12633-020-00888-2

44. Capello E, Monno M, Semeraro Q (1994) On the characterisation of surfaces obtained by abrasive water jet machining. In: Allen NG (ed) Proceedings of the 12th International Conference Jet Cutting Technology. Mech Eng Pub Ltd, London, pp 177–193

45. Wala T, Lis K (2022) Influence of selected diagnostic parameters on the quality of AWJ cutting surface. Adv Sci Technol Res J 16:129–140. https://doi.org/10.12913/22998624/144642

46. Deshpande YV, Zanwar DR, Andhare AB, Barve PS (2022) Application of ANN modelling for optimisation of surface quality and kerf taper angle in abrasive water jet machining of AISI 1018 steel. Adv Mater Process Technol 13:1–14. https://doi.org/10.1080/2374068x.2022.2096830

47. Ramesh P, Mani K (2021) Prediction of surface roughness using machine learning approach for abrasive waterjet milling of alumina ceramic. Int J Adv Manuf Technol 119:503–516. https://doi.org/10.1007/s00170-021-08052-9

48. Siddiqui TU, Shukla M, Tambe PB (2008) Optimisation of surface finish in abrasive water jet cutting of Kevlar composites using hybrid Taguchi and response surface method. Int J Mach Mach Mater 3:382. https://doi.org/10.1504/ijmmm.2008.020970

49. Gardner L, Yun X, Fieber A, Macorini L (2019) Steel design by advanced analysis: material modeling and strain limits. Engineering 5:243–249. https://doi.org/10.1016/j.eng.2018.11.026

50. Abspoel M, Scholting ME, Droog JMM (2013) A new method for predicting forming limit curves from mechanical properties. J Mater Process Technol 213:759–769. https://doi.org/10.1016/j.jmatprotec.2012.11.022

51. Ahmad J, Noor MJM, Jais MIF, Rahman ASA, Senin SF, Ibrahim A, Hadi BA (2018) Mathematical models for stress-strain curve prediction-a. AIP Conf Proc 2020:020005-1–020005-6. https://doi.org/10.1063/1.5062631

52. Pejkowski Ł, Skibicki D (2019) Stress-strain response and fatigue life of four metallic materials under asynchronous loadings: experimental observations. Int J Fatigue 128:105202. https://doi.org/10.1016/j.ijfatigue.2019.105202

53. Kale A, Singh SK, Sateesh N, Subbiah R (2020) A review on abrasive water jet machining process and its process parameters. Mater Today: Proc 26:1032–1036. https://doi.org/10.1016/j.matpr.2020.01.309

54. Yang J, Kang G, Liu Y, Kan Q (2021) A novel method of multiaxial fatigue life prediction based on deep learning. Int. J. Fatigue 151:106356. https://doi.org/10.1016/j.ijfatigue.2021.106356

55. Rusinko A, Rusinko K (2009) Synthetic theory of irreversible deformation in the context of fundamental bases of plasticity. Mech Mater 41:106–120. https://doi.org/10.1016/j.mechmat.2008.09.004

56. Rusinko A, Rusinko K (2011) Plasticity and creep of metals. Springer, Berlin

57. Rusinko A (2010) Non-classical problems of irreversible deformation in terms of the synthetic theory. Acta Polytech Hung 7:25–62

58. Valíček J, Harničárová M, Öchsner A, Hutyrová Z, Kušnerová M, Tozan H, Michenka V, Šepelák V, Mitaľ D, Zajac J (2015) Quantifying the mechanical properties of materials and the process of elastic-plastic deformation under external stress on material. Materials 8:7401–7422. https://doi.org/10.3390/ma8115385

59. Hloch S, Valicek J (2011) Prediction of distribution relationship of titanium surface topography created by abrasive waterjet. Int J Surf Sci Eng 5:152. https://doi.org/10.1504/ijsurfse.2011.041399

60. Harničárová M, Valíček J, Duer S, Kušnerová M, Palková Z, Mital'ová Z (2022) Express diagnostics of stress-strain states of materials. Materialwiss Werkstofftech 53:394–401. https://doi.org/10.1002/mawe.202100329

61. Valíček J, Harničárová M, Kopal I, Palková Z, Kušnerová M, Panda A, Šepelák V (2017) Identification of upper and lower level yield strength in materials. Materials 10:982. https://doi.org/10.3390/ma10090982

62. Valíček J, Czán A, Harničárová M, Šajgalík M, Kušnerová M, Czánová T, Kopal I, Gombár M, Kmec J, Šafář M (2019) A new way of identifying, predicting and regulating residual stress after chip-forming machining. Int J Mech Sci 155:343–359. https://doi.org/10.1016/j.ijmecsci.2019.03.007

63. Valicek J, Drzik M, Ohlidal M, Madr V, Hlavac LM (2001) Optical method for surface analyses and their utilization for abrasive liquid jet automation. In Proceedings of the 2001 WJTA American Waterjet Conference—Minneapolis, Minnesota, Minneapolis, MN, USA, pp 1–11

64. Valíček J, Harničárová M, Řehoř J, Kušnerová M, Gombár M, Drbúl M, Šajgalík M, Filipenský J, Fulemová J, Vagaská A (2020) Prediction of cutting parameters of HVOF-sprayed Stellite 6. Appl Sci 10:2524. https://doi.org/10.3390/app10072524

65. Valíček J, Borovička A, Hloch S, Hlaváček P. Method for the design of a technology for the abrasive waterjet cutting of materials (2015) U.S. Patent No. US9073175B2. Washington, DC: U.S. Patent and Trademark Office

66. Valíček J, Držík M, Hloch S, Ohlídal M, Miloslav L, Gombár M, Radvanská A, Hlaváč P, Páleníková K (2007) Experimental analysis of irregularities of metallic surfaces generated by abrasive waterjet. Int J Mach Tools Manuf 47:1786–1790

Publisher's note Springer Nature remains neutral with regard to jurisdictional claims in published maps and institutional affiliations.

Authors and Affiliations

Jan Valíček[1,2,3] · Marta Harničárová[1,2,3] · Milena Kušnerová[2] · Zuzana Palková[1,2] · Ivan Kopal[4] · Cristina Borzan[5] · Andrej Czán[3] · Rastislav Mikuš[6] · Milan Kadnár[6] · Stanislaw Duer[7] · Vladimír Šepelák[2,8]

✉ Marta Harničárová
marta.harnicarova@uniag.sk

Jan Valíček
jan.valicek@uniag.sk; valicek.jan@mail.vstecb.cz

Milena Kušnerová
kusnerova.milena@mail.vstecb.cz

Zuzana Palková
zuzana.palkova@uniag.sk

Ivan Kopal
ivan.kopal@tnuni.sk

Cristina Borzan
cristina.borzan@tcm.utcluj.ro

Andrej Czán
andrej.czan@uniza.sk

Rastislav Mikuš
rastislav.mikus@uniag.sk

Milan Kadnár
milan.kadnar@uniag.sk

Stanislaw Duer
stanislaw.duer@tu.koszalin.pl

Vladimír Šepelák
vladimir.sepelak@kit.edu

[1] Institute of Electrical Engineering, Automation, Informatics and Physics, Faculty of Engineering, Slovak University of Agriculture in Nitra, Tr. A. Hlinku 2, 949 76 Nitra, Slovakia

[2] Department of Mechanical Engineering, Faculty of Technology, Institute of Technology and Business in České Budějovice, Okružní 10, České Budějovice, Czech Republic

[3] Department of Machining and Manufacturing Technology, Faculty of Mechanical Engineering - University of Zilina, Univerzitna 1, Žilina, Slovakia

[4] Department of Numerical Methods and Computational Modeling, Alexander Dubček University of Trenčín, Ivana Krasku 491/30, Trenčín, Slovakia

[5] Faculty of Industrial Engineering, Robotics and Management Production, Technical University of Cluj-Napoca, B-dul Muncii no. 103 –105, 400641 Cluj-Napoca-Napoca, Romania

[6] Institute of Design and Engineering Technologies, Faculty of Engineering, Slovak University of Agriculture in Nitra, Tr. A. Hlinku 2, Nitra 949 76, Slovakia

[7] Department of Energy, Faculty of Mechanical Engineering, Technical University of Koszalin, 15–17 Raclawicka St., 75-620 Koszalin, Poland

[8] Institute of Nanotechnology, Karlsruhe Institute of Technology (KIT), Hermann-Von-Helmholtz-Platz 1, 76344 Eggenstein-Leopoldshafen, Germany